Two-way Eulerian-Lagrangian coupling approach in GASFLOW code for containment spray modelling

Fangnian Wang, Jianjun Xiao *, Thomas Jordan

Institute of Thermal Energy Technology and Safety (ITES), Karlsruhe Institute of Technology (KIT), Germany

ARTICLE INFO

Keywords:
Spray droplets
Condensation and evaporation
Gas mixing
Eulerian-Lagrangian approach
Computational Fluid Dynamics

ABSTRACT

Spray droplets are considered to have significant effects on the gas mixing and depressurization in the containment of nuclear power plants during hypothetical accident scenarios. The Eulerian-Lagrangian approach, which enables the two-way mass, momentum, and energy coupling of the continuous gas and the dispersed spray droplets, is promising to model the behaviours of spray droplets in 3D simulations of the full-scale containment. Two-way heat and mass transfer models have been developed in the 3D CFD code GASFLOW. The particle group method is applied in the Lagrangian approach to track the droplets. The ordinary differential equations which couple the local heat and mass exchanges between each droplet group and the surrounding gas mixtures have been solved using the Runge-Kutta method. The GASFLOW coupling this new approach is validated by TOSQAN water spray experiments, which demonstrate the good feasibility of implementing the approach. The analysis of the impact of the spray on containment atmosphere indicates that: 1) the droplet swarm entrains and mixes the surrounding gas, breaking up the gas stratification, with turbulent diffusion dominating momentum mixing in dead zones; 2) the thermal and mass exchanges between the spray droplet swarm and gas jointly determine the atmosphere depressurization, with the evaporation of the spray-formed film/sump on heat structures of great importance for the containment pressure development; and 3) these spray thermodynamic and dynamic effects highly depend on the droplet size distribution and the spray shape.

1. Introduction

During loss-of-coolant accidents in nuclear power plants (NPPs), steam is released from breaks or valves, as a result, hydrogen would be generated due to cladding oxidation (IAEA, 2011). The spray system is an emergency cooling strategy to depressurize the atmosphere, remove atmospheric heat, enhance the mixing of hydrogen, and wash-out airborne radioactive aerosols during nuclear accidents inside the containment. Spray droplet dynamics have significant impacts on steam condensation and global gas mixing in the containment atmosphere.

Numerous experimental and numerical investigations have been carried out in the past decades to study the heat and mass transfer of spray droplets in the atmosphere. Early spray experiments have been performed in large-scale facilities such as CSE (751 m^3), NUPEC (1300 m^3), and CVTR (6500 m^3) (Oecd, 1999). In the last 20 years, experiments on spray in vessels conducted in the small/intermediate-scale facilities include: TOSQAN (7 m^3), THAI (60 m^3), MISTRA (98 m^3), and PANDA (515 m^3) (Gupta et al., 2017; Malet et al., 2011a; Malet et al., 2011; Oecd, 2012). These facilities investigated the influence of spray droplets on the atmosphere that are generated via one or multiple spray nozzles. The TOSQAN facility located at the IRSN in France, THAI facility at the Becker Technologies in Germany, MISTRA facility at the CEA also in France, and PANDA facility at the PSI in Switzerland (Erkan et al., 2011; Gupta et al., 2017; Malet et al., 2011; Oecd, 2012; Porcheron et al., 2007), studied the containment depressurization due to heat and mass transfer between spray droplets and gas, and the atmosphere mixing in the containment vessel, such as the break-up of the light gas stratification caused by water spray. Although PANDA (Erkan et al., 2011) investigated the spray in two interconnected vessels, few data were published for CFD code validation. THAI (Gupta et al., 2017) and MISTRA (Oecd, 2012) also provided insights and databases for developing and validating the codes to simulate the heat and mass transfer between spray droplets and the atmosphere. However, TOSQAN (Malet et al., 2011) investigated a wider range of the spray water temperature (30–120 °C) compared to the other experiments, so the droplet evaporation was observed during the tests.

Numerical analyses of spray water droplets behaviours in the NPP

* Corresponding author at: Institute of Thermal Energy Technology and Safety (ITES), Karlsruhe Institute of Technology (KIT), Hermann-von-Helmholtz-Platz 1, 76344 Eggenstein-Leopoldshafen, Germany.
E-mail address: jianjun.xiao@kit.edu (J. Xiao).

Nomenclature

A	particle/droplet projected area on the relative velocity direction, m^2
A_p	particle/droplet surface area, m^2
A_s	wall surface area, m^2
B_m	mass Spalding number
B_T	heat Spalding number
$\boldsymbol{b}$	velocity of the control surface S, m/s
C_d	drag force coefficient
c	constant
$c_p, c_{p,v}, c_{p,g}$	water, vapor, gas specific heat capacity, J/(kg·K)
D	binary diffusion coefficient, m^2/s
d	particle/droplet diameter, m
$\overline{d}$	mean particle/droplet diameter, m
$\boldsymbol{F}_D$	drag force vector, N
$\boldsymbol{F}_b$	buoyancy force vector, N
$\boldsymbol{G}_p$	particle/droplet gravity, N
$\mathbf{g}$	gravity acceleration, m/s2
h_d/h_d^*	film evaporation/condensation coefficient/corrected one, $W/(m^{2.}{}^{\circ}C)$
h_e	droplet heat transfer coefficient, $W/(m^{2.}{}^{\circ}C)$
h_m	droplet mass transfer coefficient, $kg/(s{\cdot}m^2)$
h_w	film heat transfer coefficient, $W/(m^{2.}{}^{\circ}C)$
L_{fg}	latent heat for the droplet evaporation/condensation, J/kg
Nu	Nusselt number
n_{h_2o}	steam mole fraction in bulk
n_{s,h_2o}	steam mole fraction at the wall
Pr	Prandtl number
p	pressure, Pa
R	relaxing ratio
Re_p	particle/droplet Reynolds number
Sc	Schmidt number
Sh	Sherwood number
S_Φ	source term of the field variable Φ
S_{ρ,h_2o}, S_m, S_e	mass, momentum, energy source terms, kg/s, N·s, W
T	temperature, K
T_{surf}	particle surface temperature, K
T_∞	gas temperature in the bulk, K
T_p	particle/droplet temperature, K
t	time, s
Δt	final time step, s
Δt_g	time step of the gas flow, s
Δt_p	time step of the particle-tracking method, s
$\boldsymbol{u}_g$	gas velocity vector, m/s
$\overline{\boldsymbol{u}}_g$	gas time averaged velocity, m/s
$\boldsymbol{u}_g^{'}$	gas velocity fluctuation, m/s
$\boldsymbol{u}_p$	particle/droplet velocity vector, m/s
$\overline{\boldsymbol{u}}_p$	particle time averaged velocity, m/s
$\boldsymbol{u}_p^{'}$	particle velocity fluctuation, m/s
u^*	wall shear velocity, m/s
u^+	dimensionless velocity
V	control volume, m^3
y	vapor mass fraction
y_{surf}	vapor mass fraction on surface
α	thermal diffusivity/particles volume fraction in gas cell, m^2/s, -
δ	film thickness, m
κ	turbulent kinetic energy, m^2/s^2
κ_p	particle turbulent kinetic energy,m^2/s^2
λ_g	thermal conductivity, W/(m·K)
ζ	normally distributed numbers
$\boldsymbol{\theta}$	outward normal fractional area vector
Θ_m	correction factor of mass-transfer coefficient
μ	dynamic viscosity, Pa·s
μ_t	turbulent dynamic viscosity, Pa·s
ρ	density, kg/m^3
ρ_g	gas density, kg/m^3
ρ_p/ρ_w	particle/droplet density, kg/m^3
$\rho_{h_2o,\infty}$	steam density in the bulk, kg/m^3
$\rho_{h_2ol}^{thermo}$	liquid film density, kg/m^3
τ_p	particle response time,s

containment atmosphere have been performed with Lumped-Parameter (LP) and Computational Fluid Dynamics (CFD) codes. LP codes (e.g., MELCOR, COCOSYS, ASTEC, etc.) describe a nuclear containment as a network of control volumes/zones connected with flow paths/junctions, which can simulate the hypothetical accident scenario without providing the details of the local flow field. On the contrary, CFD codes that are capable of capturing local fields (e.g., CFX, OpenFOAM, GASFLOW, etc.) are recently preferable to investigate the containment spray phenomena. The homogeneous two-phase flow model in the serial GASFLOW code, which assumes of thermal non-equilibrium and mechanical equilibrium between the gas and droplet phases, has been used to model the spray system in the containment of NPPs (Kim et al., 2006; Movahed et al., 2005; Royl et al., 2000). These studies investigated the spray impact on hydrogen distribution in APR1400, EPR, and German reactor type Konvoi, respectively. It is also interesting and of great importance to investigate spray effect in small modular reactors (SMR) with compact equipment and less containment free volume per unit power compared to the larger water-cooled reactors (Subki, 2020). GASFLOW has been used to analyze the loss-of-coolant accident with an engineered spray system in SMR with regard to the hydrogen mitigations (Wang et al., 2022; Zou et al., 2022). The homogeneous two-phase model is an option to model the spray in both large and small nuclear containment. However, the assumption that liquid droplets are dispersed in a gaseous medium ignores the momentum coupling, which is not valid for hundred-micron droplets flowing in the atmosphere.

Recently, the approach of using the Eulerian method for the continuous gas phase and the Lagrangian method for the dispersed droplet phase has been adopted. Babić et al. (Babić et al., 2009) presented this two-way interaction approach in the CFD code CFX4.4, solving the droplet transport via the Lagrangian droplet-tracking model (incorporated in CFX via user-defined subroutines). Whang et al. (Whang et al., 2021) also implemented the Eulerian (carry gas) – Lagrangian (dispersed droplets) approach in OpenFOAM to calculate this two-phase phenomenon and analyze the effects of buoyancy and droplet size. The mass and momentum interaction between two phases were considered, but the heat and mass transfer are neglected. Ding et al. (Ding et al., 2017) developed a similar approach and implemented it into the GASFLOW code. The heat and mass transfer between the water droplets and gas were considered. However, the droplet generation characteristics and spray shape are not considered. More importantly, the spray water droplets could adhere to the surfaces of the walls and rivulets, or a film could be formed, which may largely change the total mass of the steam and the overall pressure in the confined vessel. There are few publications discussing the effect of water film evaporation on containment pressure development. Ding et al. (Ding et al., 2017) mentioned droplet-wall interaction in his simulations without describing the model and discussing the effects on the results. In these literatures, the two-way coupling approach usually assumes that

droplet-to-droplet interactions (droplet fragmentation and coalescence) are neglected due to the complexity of spray droplet collision (Foissac et al., 2011; Foissac et al., 2013; Rabe et al., 2010). Mimouni et al. (Mimouni et al., 2010) proposed a droplet-wall interaction model dedicated to the evaporation of droplets attached to a heated wall and surrounded by a hot gas. However, it is assumed that the water droplets were accumulated on the walls with a hemispherical form and then changed to steam using a symmetric extension of the nucleate boiling model. The evaporation of the water film on the walls was not considered.

The Lagrangian droplet-tracking approach is a promising method to model the behavior of water droplets produced from the spray system in 3D CFD simulations of full-scale NPP containment. However, improvements have to be implemented in a newly developed two-way coupling approach, such as full coupling of mass, momentum, and heat transfer between the gas and droplet phases instead of the homogeneous two-phase flow model, the extension of the heat and mass transfer correlations for severe accident conditions, the generated cone spray shape, and the effects of droplet-wall interaction and film evaporation. The above aspects were taken into account in the current development of GASFLOW parallel version. The effects of the droplet swarm and the film effect on the atmosphere were also analyzed with respect to the atmosphere thermodynamics and the gas stratification break-up.

2. Eulerian-lagrangian coupling approach

GASFLOW is a parallel finite-volume code based on robust computational fluid dynamics numerical techniques that solve the compressible Navier-Stokes equations for 3D volumes (Xiao et al., 2016). The generalized conservation equation is:

$$\frac{\partial}{\partial t}\int_V \Phi dV = \oint_S \Phi(\boldsymbol{b} \quad \boldsymbol{u})\cdot\boldsymbol{\theta} dS + \int_V S_\Phi dV \tag{1}$$

where V denotes the control volume, $\boldsymbol{b}$ is the velocity of the control surface S, and $\boldsymbol{u}$ is the velocity of the fluid field. The outward normal fractional area vector is denoted by $\boldsymbol{\theta}$ and is introduced by the fractional area methodology of the FAVOR algorithm. This methodology is useful in modeling variable flow areas that are involved in complex geometrical representations with greater ease and accuracy. S_Φ is the source term of the field variable Φ. The time-rate-of-change of Φ in an arbitrary control volume V is equal to the inflow of Φ through the boundary in addition to the source term. The term b - u denotes the relative velocity between the control surface and the fluid. The Lagrangian form is recovered when $\boldsymbol{b} = \boldsymbol{u}$. On the other hand, when the control volume is fixed with respect to the coordinate axes, $\boldsymbol{b} = 0$, and the Eulerian form is recovered. The Implicit Continuous Eulerian - Arbitrary Lagrangian Eulerian (ICE'd-ALE) solution algorithm is adopted. This technique is applicable to all speed flows, which means the code is valid in both sub- and supersonic flow regimes. The heat transfer mechanisms, including convective heat transfer, radiation heat transfer, heat conduction and phase change, can be modeled in the code.

2.1. Droplet-tracking

The Lagrangian droplet-tracking with the extended heat and mass transfer models have been implemented into the code. This droplet-tracking method describes the movement of the spray droplets as the spatially-dispersed phase with the following features and assumptions (Ding et al., 2017):

1. Droplet group method has been implemented into the spray model, which consists of a group of spray droplets with identical location, velocity, temperature and diameter in the same gas cell. There could be many groups of water droplets in one gas cell.
2. Two-way couplings of mass, momentum, turbulence and energy between the gas mixtures and water droplets are taken into account in the GASFLOW code.
3. Droplet-to-droplet interactions, such as droplets fragmentation and coalescence, are not considered in the current model.
4. The dispersed phase is considered to be in the form of discrete single-component rigid spherical liquid droplets.

The droplet velocity $\boldsymbol{u}_p$ is determined by the sum of the forces acting on the particle, namely the drag force $\boldsymbol{F}_D$, gravity $\boldsymbol{G}_p$ and buoyancy force $\boldsymbol{F}_b$:

$$m_p\frac{d\boldsymbol{u}_p}{dt} = \boldsymbol{F}_D + \boldsymbol{G}_p + \boldsymbol{F}_b \tag{2}$$

The gravity force and buoyancy force are combined as:

$$\boldsymbol{G}_p + \boldsymbol{F}_b = \frac{\pi}{6}d^3\mathbf{g}(\rho_p \quad \rho_g) \tag{3}$$

The shape of the liquid droplet is assumed to be spherical, so the drag force can be calculated:

$$\boldsymbol{F}_D = \frac{1}{2}C_d\rho_g A\left|\boldsymbol{u}_g \quad \boldsymbol{u}_p\right|(\boldsymbol{u}_g \quad \boldsymbol{u}_p) \tag{4}$$

where A is the droplet projected area on the velocity direction,$A = \frac{1}{4}\pi d^2$. The subscripts g and p denote gas and particle, respectively. ρ_g is the gas density. C_d is the drag force coefficient depending on particle Reynolds number (Putnam, 1961):

$$\mathrm{Re}_p = \frac{\rho_g\left|\boldsymbol{u}_g \quad \boldsymbol{u}_p\right|}{\mu_g} \tag{5}$$

$$C_d = \begin{cases} \dfrac{24}{\mathrm{Re}_p} + 4.5\mathrm{Re}_p < 5 \\ \dfrac{24}{\mathrm{Re}_p}\left(1 + \dfrac{1}{6}\mathrm{Re}_p^{2/3}\right) 5 < \mathrm{Re}_p \le 1000 \\ 0.44\mathrm{Re}_p > 1000 \end{cases} \tag{6}$$

For perfect laminar flow $Re_p < 5$, Oseen (Oseen, 1910) extended the coefficient from Stokes' law by taking the inertia terms in the Navier-Stokes equations partly into account. For turbulent wake flow $Re_p > 1000$; the drag coefficient remains approximately constant 0.44 (the so-called Newton's law for the terminal velocity). For the flow between the above two regimes $5 < Re_p \le 1000$, the coefficient is usually given by an empirical correlation, e.g. Schiller and Naumann (Schiller and Naumann, 1935) correlation currently.

The gas velocity in the definition of particle Reynolds number Re_p should take into account the turbulence effects of gas and particle, i.e.

$$\boldsymbol{u}_g = \overline{\boldsymbol{u}}_g + \boldsymbol{u}_g^{'}; \boldsymbol{u}_p = \overline{\boldsymbol{u}}_p + \boldsymbol{u}_p^{'} \tag{7}$$

where $\overline{\boldsymbol{u}}_g$, $\overline{\boldsymbol{u}}_p$ are the gas and particle time-averaged velocities given by GASFLOW solver. $\boldsymbol{u}_g^{'}$ and $\boldsymbol{u}_p^{'}$ are the velocity fluctuations of gas and particle. The turbulent dispersion can be obtained by the discrete random walk model, namely the velocity fluctuation follows the Gaussian distribution random presumptively (Gosman and loannides, 1983).

$$\boldsymbol{u}_g^{'} = \zeta\sqrt{\frac{2\kappa}{3}}; \boldsymbol{u}_p^{'} = \zeta\sqrt{\frac{2\kappa_p}{3}} \tag{8}$$

where ζ is normally distributed numbers, and κ and κ_p are the turbulence kinetic energy of gas and particle.

The droplet heat and mass transfer model is applied to estimate the evaporation/condensation rate:

$$\frac{dm_p}{dt} = \quad h_m A_p \rho_{g,\infty} ln(1 + B_m) \tag{9}$$

$$m_p c_p \frac{dT_p}{dt} = h_e A_p (T_\infty \quad T_p) + \frac{dm_p}{dt} L_{fg} \tag{10}$$

where $B_m = \frac{y_{h_2o,sat} \quad y_{h_2o,\infty}}{1 \quad y_{h_2o,sat}}$ is the mass Spalding number (Spalding, 1953); $y_{h_2o,sat}$ and $y_{h_2o,\infty}$ are the vapor mass fraction at droplet surface (saturated) and in the bulk gas, respectively. L_{fg} is the latent heat for the droplet evaporation/condensation, and A_p is the surface area of the droplet. h_e and h_m are the heat and mass transfer coefficients, respectively, which can be calculated by the Nusselt number $Nu = \frac{h_e d}{\lambda_g}$ and Sherwood number $Sh = \frac{h_m d}{D}$. D is the binary diffusion coefficient. These two dimensionless numbers can be calculated by the widely used Ranz and Marshall correlations (Ranz and Marshall, 1952):

$$Nu = 2 + 0.552 Re_p^{1/2} Pr^{1/3} \tag{11}$$

$$Sh = 2 + 0.552 Re_p^{1/2} Sc^{1/3} \tag{12}$$

However, it has been found that Ranz and Marshall correlations (Ranz and Marshall, 1952) could overestimate the transfer rate at low Reynolds number ($Re_p \leq 10$). As an alternative, the Clift correlation (Clift et al., 1978) is recommended when $Re_p \leq 400$. Furthermore, the subcooling droplets could be surrounded by a high-temperature atmosphere during severe accidents. It has been reported in previous studies that the expected high rate of phase change would reduce the droplet heat and mass transfer (Amani and Nobari, 2013; Zhifu et al., 2013). An uniform formulation based on Ranz and Marshall correlations with a correction factor, is highlighted in our previous work (Wang et al., 2023) as follows:

$$Nu^* = (1 + B_T)^{-2/3} \left(1 + (1 + Re_p Pr)^{1/3} max\left(1, Re_p^{0.077}\right)\right) \tag{13}$$

$$Sh^* = (1 + B_m)^{-2/3} \left(1 + (1 + Re_p Pr)^{1/3} max\left(1, Re_p^{0.077}\right)\right) \tag{14}$$

where B_T is the heat Spalding number. B_T is a function of B_m(Abramzon and Sirignano, 1989; Strizhak et al., 2018), which can be computed as $B_T \approx (1 + B_m)^{\left(\frac{\rho_g D c_{p,v}}{\lambda_g}\right)} \quad 1$. $c_{p,v}$ is the vapor specific heat capacity, and $Le = \frac{\lambda_g}{\rho_g D c_{p,g}}$ is the Lewis number. $Pr = \frac{\mu_g C_p}{\lambda_g}$ and $Sc = \frac{\mu_g}{\rho_g D}$ are the gas Prandtl number and Schmidt number, respectively. The "1/3 rule" is used to estimate the droplet surface temperature T_{surf}, and the vapor mass fraction y_{surf}:

$$T_{surf} = T_p + \frac{1}{3}(T_\infty \quad T_p) \tag{15}$$

$$y_{surf} = y_{h_2o,p} + \frac{1}{3}(y_{h_2o,\infty} \quad y_{h_2o,p}) \tag{16}$$

It is recommended in Ref. (Yuen and Chen, 1976) to use y_{surf} to calculate the thermal properties in the thin gas layer around the droplet surface. The vapor mass fraction at the droplet surface $y_{h_2o,p}(T_p)$ is obtained when the droplet temperature is given.

The coupled mass and energy ordinary differential equations are solved using the Runge-Kutta method. The location, diameter, velocity and temperature of each droplets group will be updated. The contributions of each droplets group to the continuous phase are served as the source terms S_Φ in the mass, momentum and energy conservation equations *Eq. (1)* of the gas phase, i.e.

$$S_{\rho,h_2o} = \quad \sum \frac{dm_p}{dt} \tag{17}$$

$$S_m = \quad \sum \boldsymbol{F}_D dt \tag{18}$$

$$S_e = \quad \sum m_p c_p \frac{dT_p}{dt} + \sum \frac{dm_p}{dt} L_{fg} \tag{19}$$

The maximum residuals of the droplet diameter, temperature and velocity are converged to 10^{-5}, 10^{-5} and 10^{-3}, respectively. The time step of the particle integration Δt_p is the minimum of the element length scale over the particle speed. The global time step for the transient gas flow Δt_g is subject to the Couran-Friedrichs-Lewy (CFL = 0.25 default) number. The adopted time step for both gas and particle phases $\Delta t = \min(\Delta t_g, \Delta t_p)$.

2.2. Spray droplets' generation

Water spray creates multiple droplet clouds, with each cloud representing a group of droplets possessing equal characteristics such as position, velocity, size, and temperature. The droplet clouds are generated in each time step with a specific spray water injection rate and a user-defined simulation droplet number. The initial droplet temperature is the same as the spray injection temperature. The size of the droplets is determined by selecting a droplet diameter d from a log-normal distribution, which is the single-tailed probability distribution with a droplet mean diameter $\bar{d}$ and variance σ^2 as follows (Erkan et al., 2011):

$$f(d) = \frac{1}{\sqrt{2\pi}\sigma d} exp\left(\frac{(ln(d/\bar{d}))^2}{2\sigma^2}\right) \tag{20}$$

In reality, the size distribution is associated with the type of spray nozzle and injection pressure. High injection pressure could generate droplet sizes with smaller deviation, and vice versa. The spray droplets are generated randomly in a used-defined zone where the spray nozzle installed in the containment. The input deck should include information regarding the injection location, diameter, velocity, and number of droplets in each droplet class.

The shape of the spray is determined by the type of nozzle used. Fig. 1 shows two types of sprays used in industries that generate a full or hollow cone spray (the spray experiment images are extracted from (Foissac et al., 2011). The spray shape and size distribution in the spray area close to the nozzle seem to be independent of the distance from the nozzle. The droplet velocity consists of an axial and radial component, while the swirl created by the nozzle is attenuated very quickly in the first few centimeters from the nozzle. In a full cone spray, as seen in Fig. 1 (a), the droplets are distributed homogeneously throughout the entire spray section, which can be divided into several annular sections that represent the Gaussian velocity distribution on the spray section. In a hollow cone spray, as seen in Fig. 1 (b), most of the droplets are concentrated in an annular spray section, and a maximum water mass is present in the middle area, which can also be approximated as a Gaussian distribution.

2.3. Spray-Wall interaction and water film evaporation

Water spray can create rivulets and film on walls, and sumps in the containment cavity. A heat transfer model of spray-wall interaction was developed and implemented in GASFLOW with the following assumptions:

- A water film is formed as soon as the water droplets adhere on the wall surfaces. Only water film evaporation on the walls is considered, and boiling or evaporation of the water droplets and rivulet on the walls is not modelled.
- A critical water film thickness is used. The extra water above the critical thickness will be moved directly to the sump. Water evaporation and steam condensation could occur on the surface of the water sump.

Phase changes can occur between gas and structures on any surface within the containment, including walls, ceilings, floors, and internal structures. Such phase changes can occur under either of two conditions

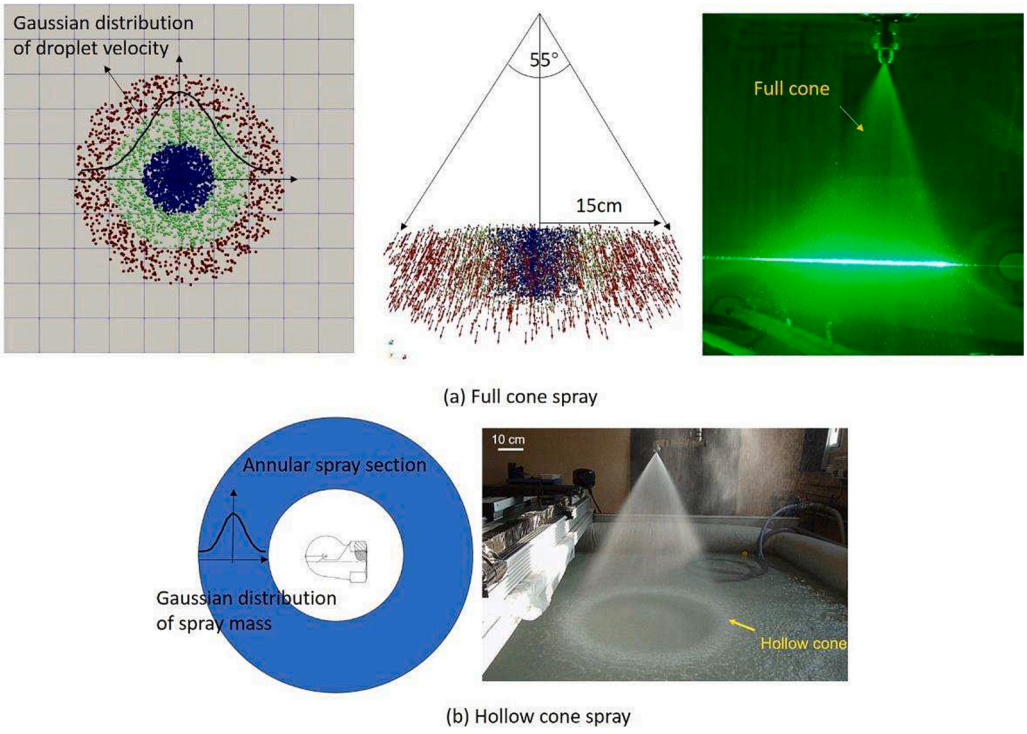

Fig. 1. Full and hollow cone spray shape.

(Xiao et al., 2016b): (1) when the surface temperature is lower than the saturation temperature of the water vapor present near the surface, leading to condensation, or (2) when condensate is already present on a given structural surface, and the temperature of the condensate surface is higher than the saturation temperature of the gas mixture adjacent to the surface, leading to vaporization. The rate of phase change on a structural surface can be described as follows:

$$\dot{m}_s = h_d^* A_s \left(\rho_{\mathrm{h_2o}} \quad \rho_{s,\mathrm{sat}}\right) \tag{21}$$

where h_d^* is the corrected mass-transfer coefficient, $\rho_{\mathrm{h_2o}}$ is the water vapor density in the gas mixture, and $\rho_{s,\mathrm{sat}}$ is the saturation water vapor density at the structural surface. The saturation density is computed from the saturation pressure and the structural surface temperature $\rho_{s,\mathrm{sat}} = \frac{p_{s,\mathrm{sat}}(T_s)}{R_{\mathrm{h_2o}} \cdot T_s}$, where the saturation pressure is evaluated as a function of temperature from the integrated Clausius-Clapeyron equation $p_{\mathrm{sat}}(T) = 10^6 \cdot e^{\frac{c_1 + c_2 \cdot T}{c_3 \cdot T}}$. The mass-transfer coefficient can be expressed in terms of the heat-transfer coefficient,

$$h_d = \frac{h_w}{\rho c_p} \left(\frac{Sc}{Pr}\right)^{-\frac{2}{3}} \tag{22}$$

by using the Chilton-Colburn empirical analogy between heat and mass transfer. The Reynold analogy is adopted for calculating the heat-transfer coefficient,

$$h_w = \frac{\rho c_p u^*}{u^+} Pr^{-\frac{2}{3}} \tag{23}$$

where u^* is wall shear velocity and u^+ is dimensionless velocity, $u^+ = u_c/u^*$, u_c is cell-center fluid velocity. Following similar ideas as with the heat-transfer coefficient for relatively large steam mass fractions, the mass-transfer coefficient is corrected by

$$h_d^* = \Theta_m h_d \tag{24}$$

where $\Theta_m = \frac{\log(R+1)}{R}$, and the relaxing ratio R is expressed as $R = \frac{\frac{n_{s,\mathrm{h_2o}} \quad n_{\mathrm{h_2o}}}{1 \quad n_{s,\mathrm{h_2o}}}}{}$. $n_{s,\mathrm{h_2o}}$ is the steam mole fraction at the wall, and $n_{\mathrm{h_2o}}$ is the steam mole fraction in the gas mixture.

For the situation where "dryout" of a surface may occur, i.e., the liquid film totally evaporates leaving the surface dry, a better formulation of the surface mass transfer equation is

$$\dot{m}_s = max\left[\frac{\delta A_s \rho_{\mathrm{h_2ol}}^{\mathrm{thermo}}}{2\Delta t}, h_d^* A_s \left(\rho_{\mathrm{h_2o}} \quad \rho_{s,\mathrm{sat}}\right)\right] \tag{25}$$

where δ is the film thickness. Note that a positive sign in the equation indicates condensation, while a negative sign signifies vaporization of the liquid film. At the point of near dryout, we only allow half of the available film to evaporate in a given time step. The total mass source or sink term due to phase change involving structural surfaces in gas conservation equations for all surfaces will then be calculated.

$$\int_V S_{\rho,\mathrm{h_2o,condensation/vaporization}} dV = \sum_s max\left[\frac{\delta A_s \rho_{\mathrm{h_2ol}}^{\mathrm{thermo}}}{2\Delta t}, h_d^* A_s \left(\rho_{\mathrm{h_2o}} \quad \rho_{s,\mathrm{sat}}\right)\right] \tag{26}$$

3. Validations by one single droplet experiments

To validate the Lagrangian droplet-tracking approach in GASFLOW (Wang et al., 2023); we first tested the velocity of a free-falling droplet without heat and mass transfer. The terminal velocities of water droplets with various sizes falling in stagnant air measured by Gunn and Kinzer (Gunn and Kinzer, 1949) were compared with the calculated results with a very small deviation (maximum of discrepancy of 0.2%). This indicates that the momentum prediction of droplets-gas coupling has good agreement with the analytical solution and measurement data.

Next, we investigated a GASFLOW simulation (Wang et al., 2023) of the evaporation dynamics of an isolated, stagnant droplet in dry air and compared it with the experiment of Ranz and Marshall (Ranz and Marshall, 1952). The simulation results, analytical solution, and experimental data showed excellent agreement. The current heat and mass transfer correlations are valid for a wide range of spray droplet sizes, from 50 μm to 1000 μm.

The mass, momentum, and heat transfers of a single droplet were investigated in the IRSN CARAIDAS experiment (Malet et al., 2011a; Plumecocq and Passalacqua, 2001) under typical post-accident atmosphere conditions. The behaviors of a single droplet revealed good agreements in the comparisons between the approach predicted and the experimental data (Wang et al., 2023), although uncertainties still exist in droplet evaporation tests with a large phase change rate.

However, the simulation of a single droplet only reveals one-way coupling results. Therefore, it is necessary to simulate a spray droplet swarm in the atmosphere to validate the newly developed two-way coupling approach.

4. Validations by integral spray experiments

4.1. TOSQAN spray experiments and GASFLOW modelling setup

The heat and mass transfer of a single droplet has a very slight influence on the temperature, pressure, and gas concentration in the atmosphere. The quantity of heat and mass transfer is too small to significantly vary the global or local temperature. The current Eulerian-Lagrangian two-way coupling approach considers the sum of multiple droplets' effects as source terms in the continuous gas phase equations.

There are two major impacts of spray multiple droplets on the atmosphere: the dynamic (gas entrainment and mixing) and thermodynamic (steam condensation and droplet evaporation) effects of the spray. To investigate these phenomena, spray experiments were performed in the TOSQAN facility (Malet et al., 2011; Porcheron et al., 2007), as shown in Fig. 2 (a). The cylindrical vessel has a volume of 7 m^3, is 4.8 m high, and has an internal diameter of 1.5 m. The spray system is located 0.65 m from the top of the enclosure on the vertical axis, which produces a full cone (spray angle 55°) water spray, as seen in Fig. 1 (a). Gas temperature is measured by thermocouples, and gas concentration is measured by mass spectrometry and Raman spectroscopy. Droplet velocity and size distribution are measured by PIV and visualization techniques (Porcheron et al., 2002).

The reference GASFLOW mesh with 32 × 32 × 98 cells (cell length Δx = 5 cm, red points are the measurement locations) is presented in Fig. 2 (b). The coarse (cell length Δx = 10 cm) and fine mesh (cell length Δx = 2.5 cm) are also utilized for the mesh independence analysis, as shown in the results in the supplementary data. These results indicate that the reference mesh is acceptable for simulations with regard to calculation accuracy and time consumption.

The TOSQAN 113 test investigated the mixing of the atmosphere in the containment vessel, which was initially filled with air-helium, and the break-up of the helium stratification caused by the spray effect. Helium, which is a light gas, is usually used to simulate the burnable gas hydrogen in experiments due to safety concerns. Prior to the test, compressed air is injected into the vessel to clean the remaining gas mixture from previous tests. Then, the vessel is closed, and helium is injected radially, at a mass flow rate of around 1 g/s at the top of the dome. When the vessel pressure reaches 2 bar (temperature around 30 °C), the helium injection is stopped. After a delay to establish the helium stratification, the spray is activated. The atmosphere becomes homogeneous after several hundred seconds and reaches a steady state at the end of the test. The characteristics of the spray injection and the initial conditions are given in Table 1 and Table 2. However, in reference to Movahed and Travis (Movahed and Travis, 2010), the full calculation (pre-calculation before spray) provided valuable insights for obtaining

Table 1
Spray injection characteristics.

	TOSQAN 101	TOSQAN 113
Spray mass flow rate	29.96 g/s	30.0 g/s
Spray angle	55°	55°
Injected water temperature (linear interpolation between two steps)		
at t = 0 s	119.1 °C	30 °C
at t = 311 s	22.1 °C	
at t = 1000 s	27.7 °C	
Droplet mean diameter d_{10}	145 μm	137 μm
Initial droplet velocity	~10 m/s	~10 m/s

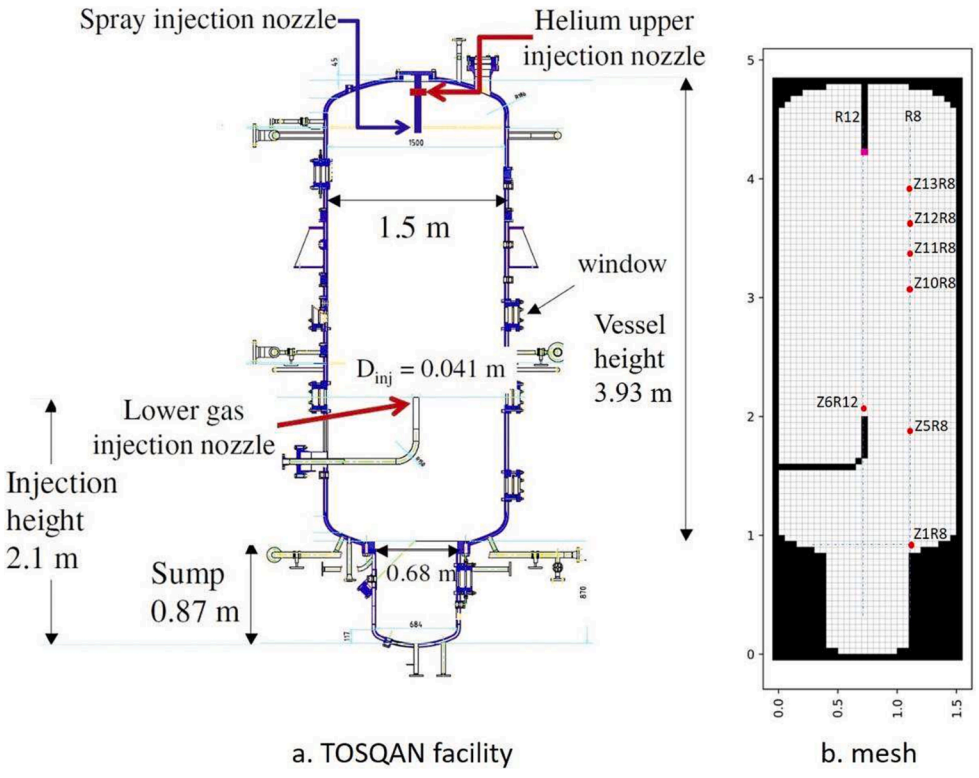

Fig. 2. TOSQAN experiment facility (Malet and Huang, 2015) and GASFLOW mesh.

Table 2
Initial conditions before spray.

TOSQAN 101	TOSQAN 113	
Elevation* / steam concentration	Elevation / Helium concentration	Elevation / Gas temperature
4.8 m / 70%	3.97 m / 99%	3.97 m / 31.8 °C
–	3.13 m / 85.8%	3.13 m / 36.9 °C
–	2.8 m / 47.6%	2.67 m / 34.7 °C
–	1.9 m / 2.3%	2.04 m / 30.1 °C
0.87 m / 10%	0.87 m / 1.9%	1.2 m / 28.7 °C

Note: *elevation from the vessel bottom.

accurate boundary conditions, such as temperature and gas distributions prior to the spray. Instead of initializing conditions homogeneously in the vessel, a full simulation of the TOSQAN 113 test is performed, which considers the pre-helium injection phase resulting in the gas stratification in the containment, and then the calculations with various droplet sizes and spray shapes are restarted at the moment of spray activation.

The TOSQAN 101 air–steam initialized spray test was aimed at investigating atmosphere depressurization due to heat and mass transfer between spray droplets and gas. At the beginning of the TOSQAN 101 test, the vessel is filled with air (1 bar and 120 °C). Superheated steam (151 °C, 13 g/s) is then injected from the lower nozzle into the vessel until the atmospheric condition reaches 2.5 bar of pressure, 131 °C of temperature, 213 mol of air, and 308 mol of steam (average steam concentration 59.1 vol%). The vessel walls, which are heated with oil, have a sufficiently high temperature to prevent steam condensation. The walls are insulated, and the wall temperatures are not uniform but rather quite similar, at around 120 °C (see Tab. 2 in ref. (Malet et al., 2011). After the steam injection, the spray starts at 4.15 m elevation on the vessel axis with a mass flow rate of approximately 30 g/s. The characteristics of the spray injection are given in Table 1. Due to the upward steam injection in Test 101 at the 2.1 m vessel elevation before the spray, a steam molar fraction variation in the vertical direction is measured during the experiment, as shown in Table 2. To obtain the boundary condition before the spray, a full simulation that considers the pre-steam injection is performed, rather than a simulation that initializes homogeneously with temperature and steam concentration. In both Test 113 and Test 101, the data in Table 2 are used to verify the accuracy of the pre-calculations before the spray.

The spray droplets are generated in a cylindrical zone, occupying at least one cell in height (rather than a planar surface). This zone is situated at a specific distance from the nozzle and initialized with experimental data encompassing size and velocity distributions. In the simulations of TOSQAN spray experiments, as depicted in Fig. 1 (a), the spray is implemented within a 10 cm high zone located 5 cm below the spray nozzle. The bottom surface of the spray zone has a circular radius of 15 cm. The spray angle 55° determines the direction of droplet velocities. The velocity distribution on the spray section is represented by three annular sections with velocities of 10 m/s (center), 8 m/s, and 6 m/s, respectively, as derived from experimental data (Porcheron et al., 2007). Fig. 3 presents the TOSQAN spray droplet size distribution. The droplet number follows a log-normal distribution (Malet et al., 2005). The corresponding mass fraction is reconstructed by knowing the droplet size and number. A bigger size droplet has a larger mass fraction despite a smaller droplet number. The mass fraction of each droplet size is used to distribute the spray mass to each droplet cloud. From the perspective of heat and mass transfer, using the Sauter mean diameter of droplets seems like an alternative to the geometric mean diameter. The Sauter mean diameter is defined as the diameter of a sphere that has the same volume-to-surface area ratio as a particle of interest. The Sauter mean diameter is obtained by its definition: $d_{32} = 6\frac{\sum V_p}{\sum A_p} = 212\,\mu$m. The numerical information used in GASFLOW modelling is summaried in Table 3.

Table 3
Numerical information in GASFLOW modelling.

Turbulence model	κ ε model	
Advection scheme	Van Leer, 2nd order	
Mesh	TOSQAN 101 Cylindrical, cell length Δx = 3 cm	TOSQAN 113 Cartesian, cell length Δx = 5 cm
CFL number	2.5	2.5
Time step	automatic time step control Initial 10^{-4}	Initial 10^{-3}
Gas conditions	Pre-calculation before spray	
Wall temperature	Time-dependent table	

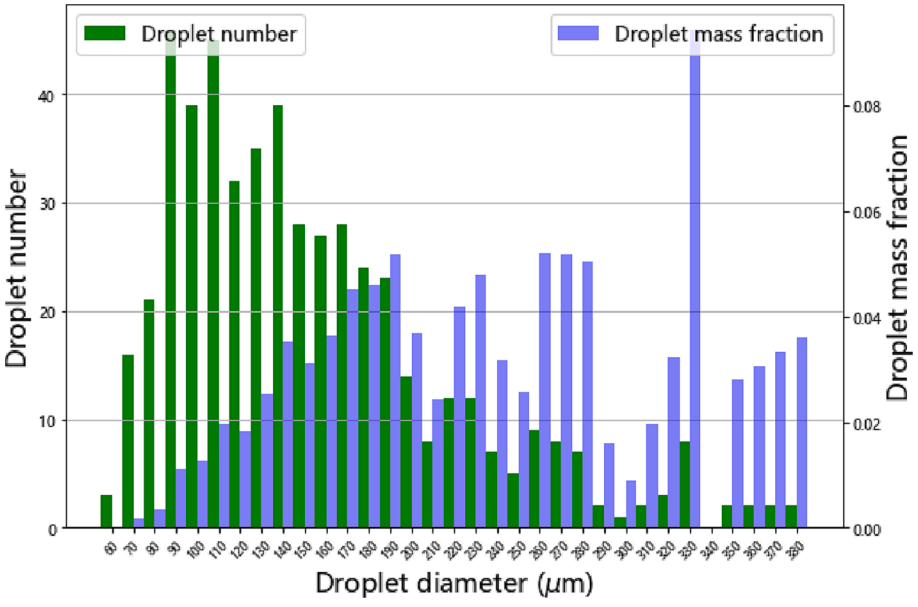

Fig. 3. Tosqan spray droplet size distribution.

4.2. Gas mixing driven by spray droplets in TOSQAN test 113

4.2.1. Gas mixing

The simulation of TOSQAN 113 test was performed to investigate how spray entrains and mixes gas to break up the light gas stratification in the containment vessel. The evolution of helium distribution in the test vessel over time is illustrated in Fig. 4. The image at time t = 0 s was obtained by pre-calculation of the helium injection phase, which is consistent with the boundary conditions given in Table 2. After the spray activation, the gas entrainment caused by droplet injection resulted in the erosion of the helium stratification. This erosion developed downwards and upwards, and definitely the downward erosion was much more intensive than the upward one in the current case due to the downward water spray. The zone above the nozzle appeared as a 'dead' zone since the velocity there was too small to mix the gas effectively. The gas in the 'dead' zone was mainly eroded by diffusion. At the end of the test, the gas was mixed very well below the spray nozzle, and it could be expected that the gas concentration would be homogeneous throughout the vessel if the spray continued long enough.

The shape of the droplet number concentration in the test vessel, as shown in Fig. 5, revealed that modified GASFLOW was feasible to model the engineered spray nozzles to initialize droplet generation and spray shape. Initially, a full cone spray was generated, but the size of the cone became smaller due to the gas flow effect. It appeared that only the area of the nozzle exit maintained the cone shape, and the shape of the droplet swarm in the lower part appeared as a cylinder. The change in spray shape could be explained by the development of the velocity vector and gas entrainment in the test vessel, as shown in Fig. 6. At the very beginning of the spray, the droplets dragged the gas to flow downwards, then two flow circulations yielded both in the upper and lower vessel. The gas in the upper part generally flowed from the wall to vessel center, which decreased the radial component of droplet velocity. Thus, the droplet swarm shape became cylindrical. Interestingly, the helium-air interface was located between the two layers of circulated convections, consequently, the droplets dispersed radically around the interface. These results were exactly as expected with the Eulerian-Lagrangian two-way coupling approach.

4.2.2. Effects of droplet size and spray shape

The evolutions of helium volume fraction at different heights with droplet size effect are presented in Fig. 7. All calculations consider the injected droplet velocity profile with a Gaussian distribution. The results of the reference case with a log-normal droplet size distribution and full cone spray shape agree well with the experimental data. The geometric mean diameter $d_{10} = 137$ μm and Sauter mean diameter $d_{32} = 212$ μm are used instead of the droplet size distribution to observe the droplet size influence. The comparison with various droplet sizes generally shows that the results of the reference case have the best agreements with experimental data. The droplet size distribution has a small influence on the upper helium stratification, as seen in the measurements of Z13, Z11, and Z10. The biases mainly remain in the measurements of Z5 and Z1 in the lower part of the test vessel. In these two locations, a large concentration gradient occurs due to the gas entrainment by the spray. It can be seen that the spray with a smaller diameter d_{10} mixes the gas more strongly than the one with a larger diameter d_{32}, so that the helium is entrained earlier from the upper part to the lower part.

The sum of the drag force of the droplets with terminal velocity is actually independent of the droplet size since the spray mass flow is identical in each calculation, and each droplet's drag force equals its gravitational force. However, the small droplet has a small terminal velocity (Wang et al., 2023), so that the smaller droplet with an identical initial velocity needs a larger or longer drag to be decelerated to its terminal velocity. This demonstrates the importance of the small spray droplet size in obtaining good gas entrainment in the lower part of the vessel. Additionally, it seems that the helium concentration in the lower part increases at a very later time, since the turbulent diffusion rather than the convective flow dominates the gas mixing there. The turbulent diffusion coefficient surely depends on the turbulence model (κ ε model used here) but also the modeling mesh effect because of the numerical error, as shown in the supplementary data, which indicates that the main deviations between the results of reference and fine meshes are located in the lower part of the test vessel.

The calculations with a full and hollow cone spray shape respectively are performed to investigate the shape effect, as shown in Fig. 8. These two calculations have an identical spray mass flow rate, droplet size distribution, and velocity profile. However, the area of the spray section is quite different. The case of the hollow cone spray has worse gas entrainment than the full one since the area of the hollow cone spray section is smaller. The helium is entrained into the middle height of the vessel at the beginning of the spray, but the entrainment slows down in the lower part. The measurement Z10R8 is an example to depict the deviation. Actually, there is an even higher bias at lower locations since the helium arrival there is delayed a lot in the case of the hollow cone spray.Fig. 9.

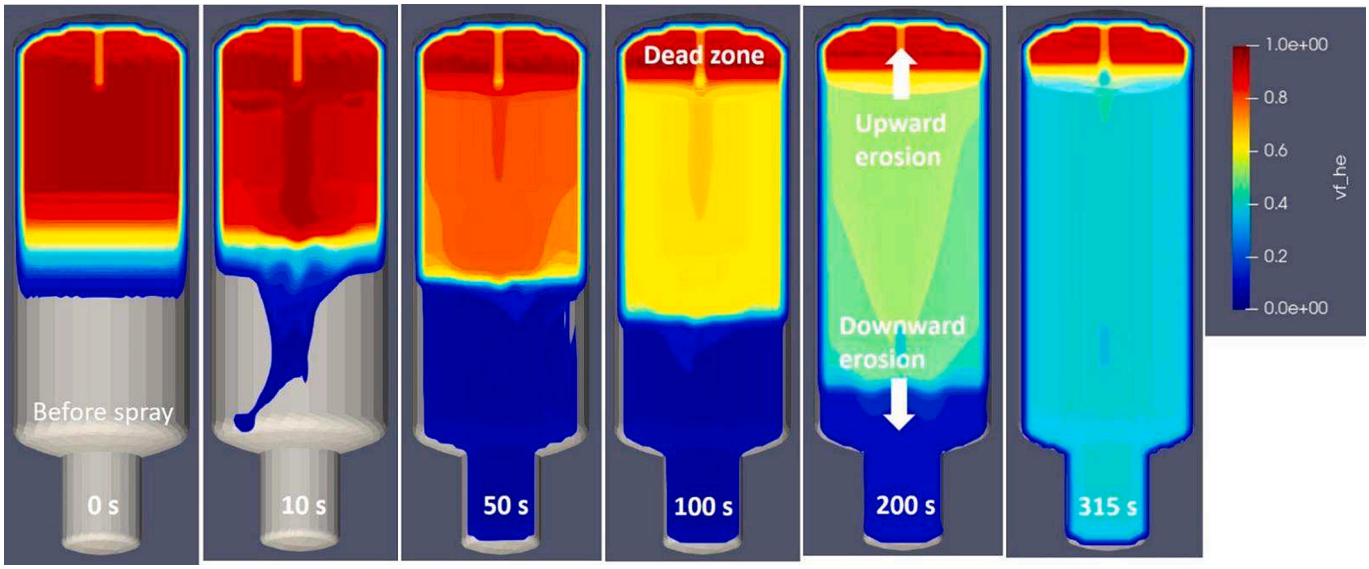

Fig. 4. Helium distribution in test vessel.

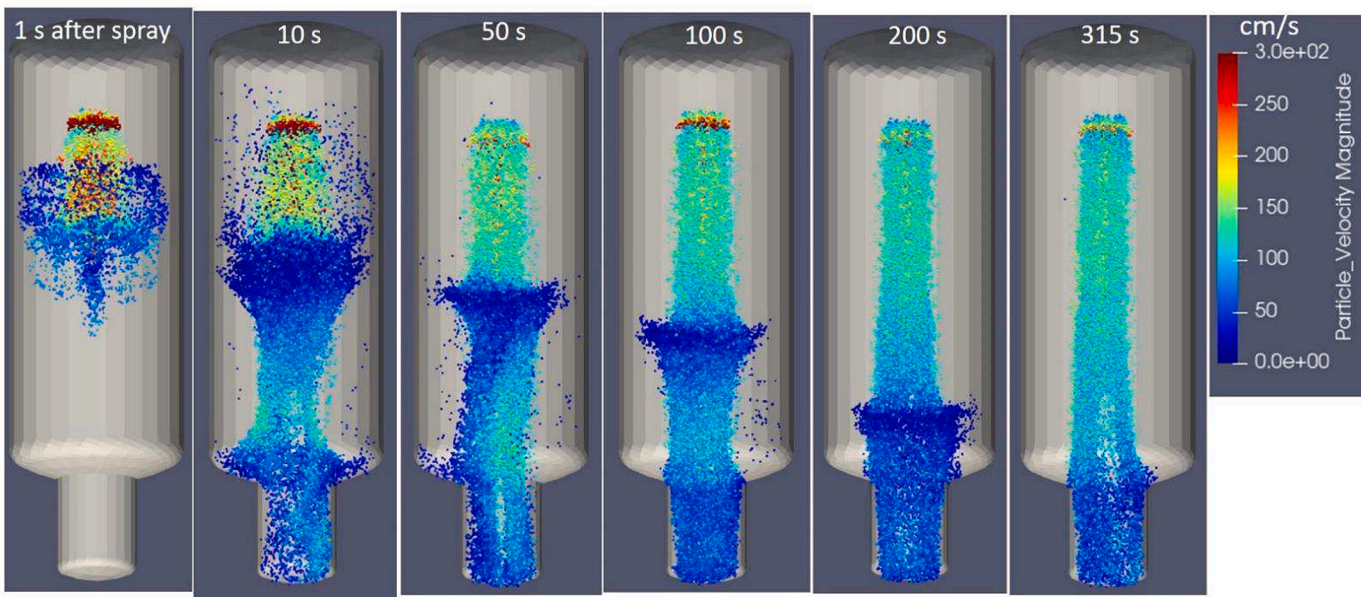

Fig. 5. Droplet distribution in test vessel.

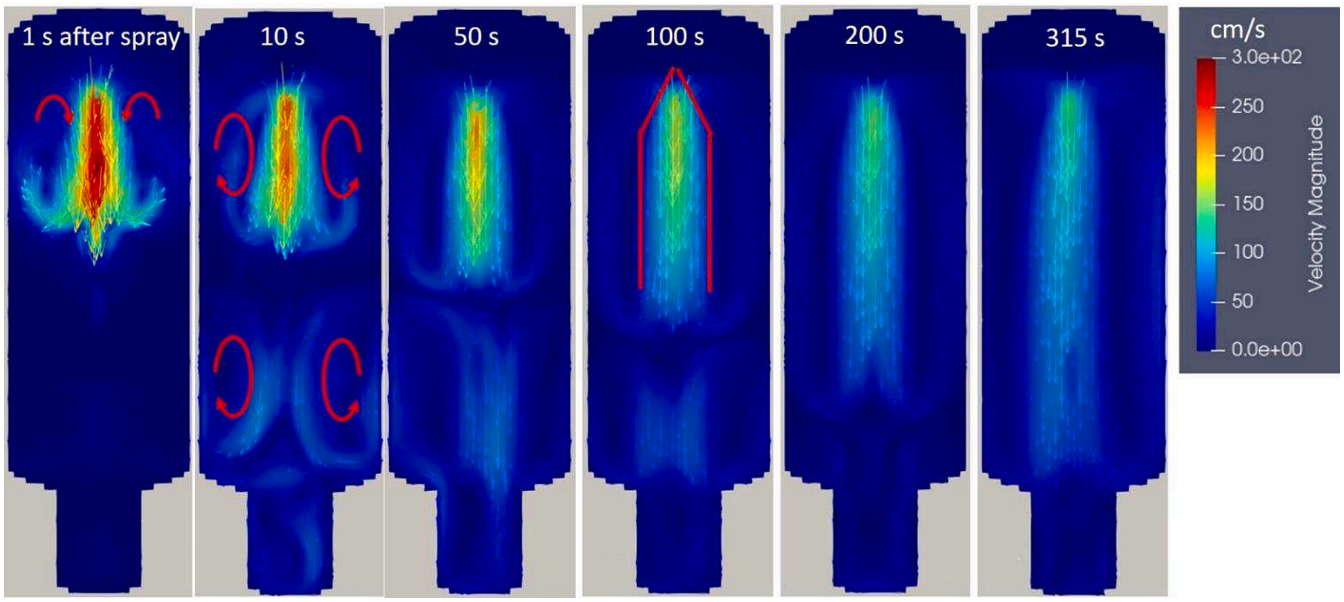

Fig. 6. Velocity vector in test vessel.

4.3. Thermohydraulic effects of spray droplets in TOSQAN test 101

4.3.1. Initial and boundary conditions

Previous simulations (Babić et al., 2009; Ding et al., 2017) assumed that the atmosphere inside the vessel consisted of an air–steam mixture with 70% and 10% steam in the upper and lower parts of the TOSQAN facility, as presented in Table 2. However, it has been found that this assumption differs substantially from the conditions of the experiment (Malet et al., 2011; Porcheron et al., 2007). This discrepancy may introduce uncertainties and errors into the results of the numerical simulation. Therefore, the simulation of the steam injection phase has been performed to establish the initial conditions of temperature and steam concentration in the experimental vessel.

Fig. 12 illustrates the calculated temperature of the air–steam mixture (left side) and steam volume fraction (right side) before the spray activation, respectively. Qualitatively similar results were obtained from the experimental data by Refs. (Lemaitre et al., 2005; Mimouni et al., 2010). The temperature and volume fraction fields were found to be non-uniform. The high-temperature area is located under the steam injection nozzle, which is consistent with the interface of steam stratification. The development process of temperature and water vapor concentration is synchronous. The steam released upwards and compressed the interface of gas stratification downwards under the release location at 2.1 m height, leading to an increase in temperature in that area. The maximum gas temperature difference is over 40 °C, which can significantly affect various heat transfers between the droplets and gas. The steam concentration generally separates into two parts, in agreement with the data in Table 2. However, the simulation shows an obvious transition region of approximately 1 m height under the steam release location. After the spray activation, droplets could enter into a dry and hot area, leading to rapid vaporization for approximately a hundred seconds. Direct entrainment by the spray would be the primary

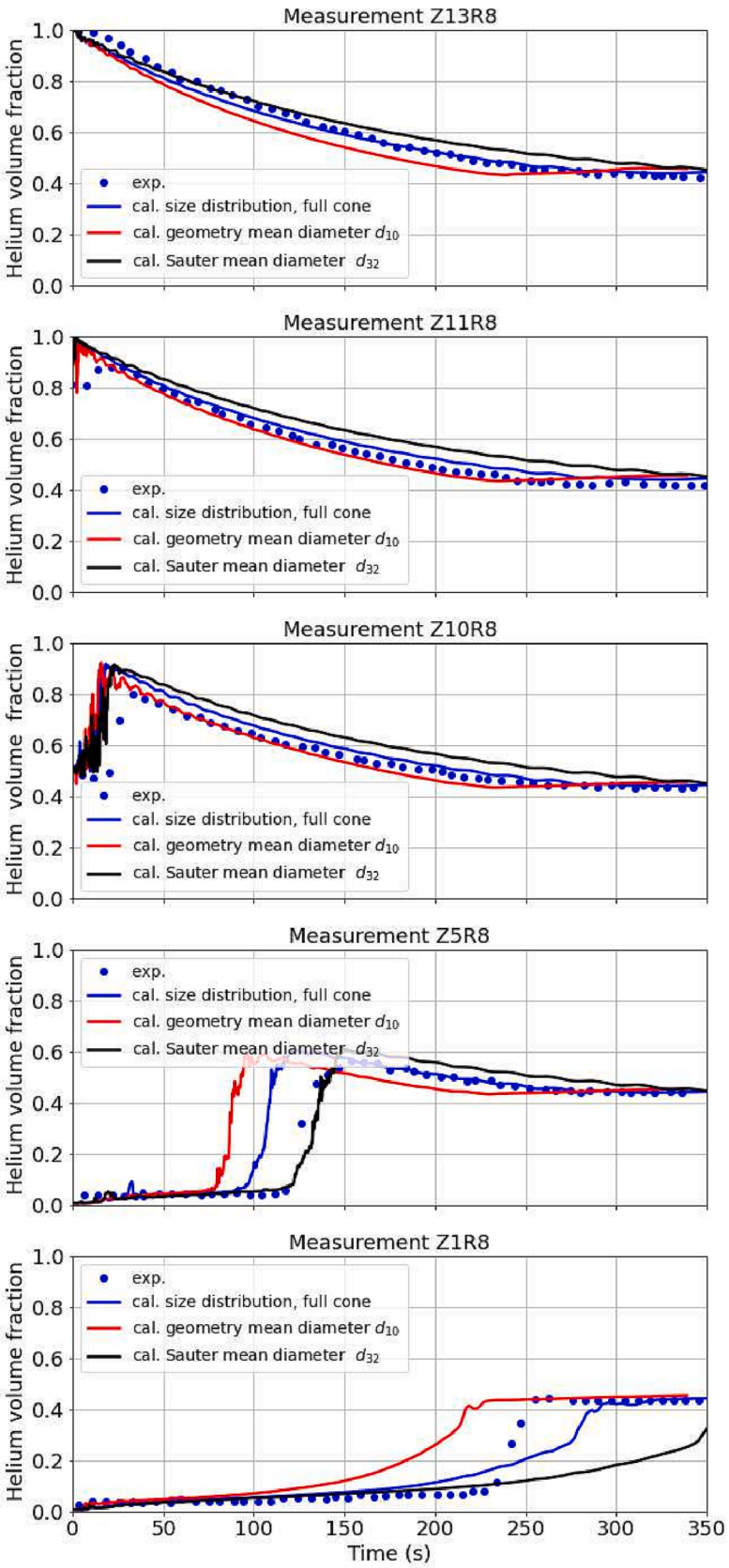

Fig. 7. Spray droplet size effect on gas mixing.

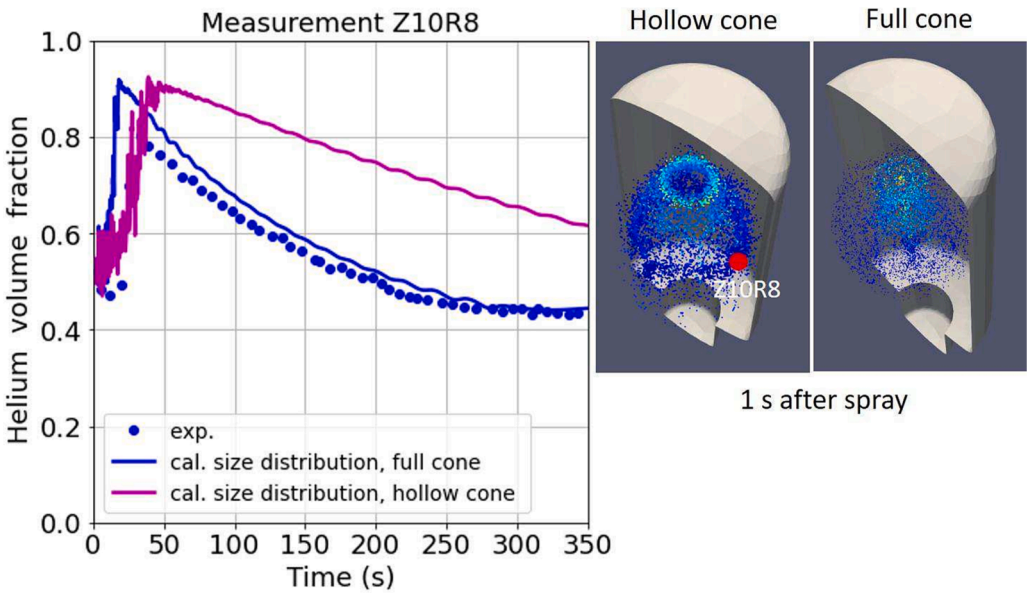

Fig. 8. Spray shape effect on gas mixing.

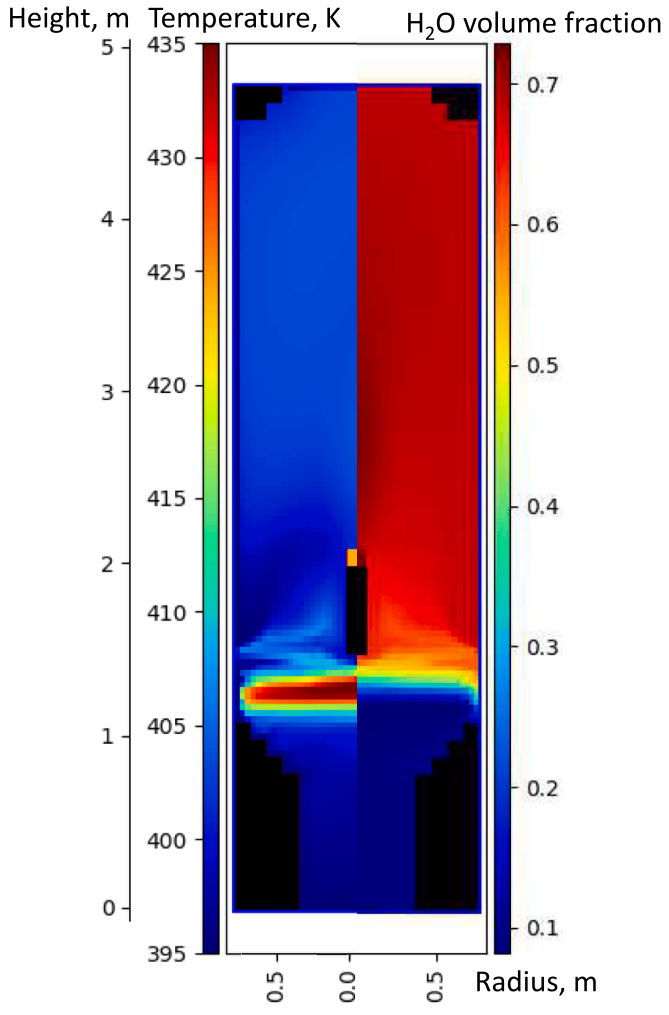

Fig. 9. Gas temperature and steam volume fraction before spray.

dynamic phenomenon during this stage. Therefore, the initial stratification of temperature and steam concentration could significantly affect the droplet heat and mass transfer at the beginning of the spray, which is of great importance for simulating the thermodynamics of the spray impact on the atmosphere.

4.3.2. *Pressure and temperature evolutions*

The simulation of the TOSQAN 101 test was performed to investigate the effects of spray droplets on the thermodynamics in the facility. Fig. 10 presents the comparisons of three global parameters over time: pressure, average gas temperature, and total gas mole number in the TOSQAN vessel for the full calculation, including the simulation of the pre-steam injection phase. The comparison of the calculated results with the measured experimental results shows good agreement in all five phases, namely, the pre-steam injection, droplet (and film) evaporation, steam fast condensation phase, steam slow condensation, and finally, the steady-state equilibrium phase. The maximum deviations are less than 10% for all three global values, which occur during the evaporation phase due to uncertainties from the evaporation of high-temperature droplets and film on walls. The temperature of the water spray is so high (119 °C) that the superheated gas may heat the droplets, probably up to the boiling temperature. When the droplet temperature reaches the boiling point, a boiling rate equation in the heat transfer model should be applied using a modified $B_m = \frac{c_{p,\infty}(T_\infty - T_p)}{L_{fg}}$.

Considering the contributions of the pressure increase due to the droplets and film evaporation and decrease due to the gas cooling by water droplets, the depressurization rate due to the mass exchange and the thermal exchange can be obtained using the ideal gas law:

$$\frac{dP}{dt} = \frac{R}{V}\left(T\frac{dn}{dt} + n\frac{dT}{dt}\right) \tag{27}$$

where $\frac{dn}{dt}$ and $\frac{dT}{dt}$ represent the rate of mass exchange and the thermal exchange, whose contributions to pressure change, are plotted in Fig. 10. It can be seen that the both mass and thermal exchanges affect the pressure positively (increase the pressure) at the beginning of the spray, but the mass (steam) exchange dominates the gas depressurization rate during the whole test process. The positive effect is balanced by the negative effect of mass (steam) exchange afterward. Finally, a steady-state is obtained since neither thermal nor mass exchange occurs anymore.

The measured average temperature was obtained from limited

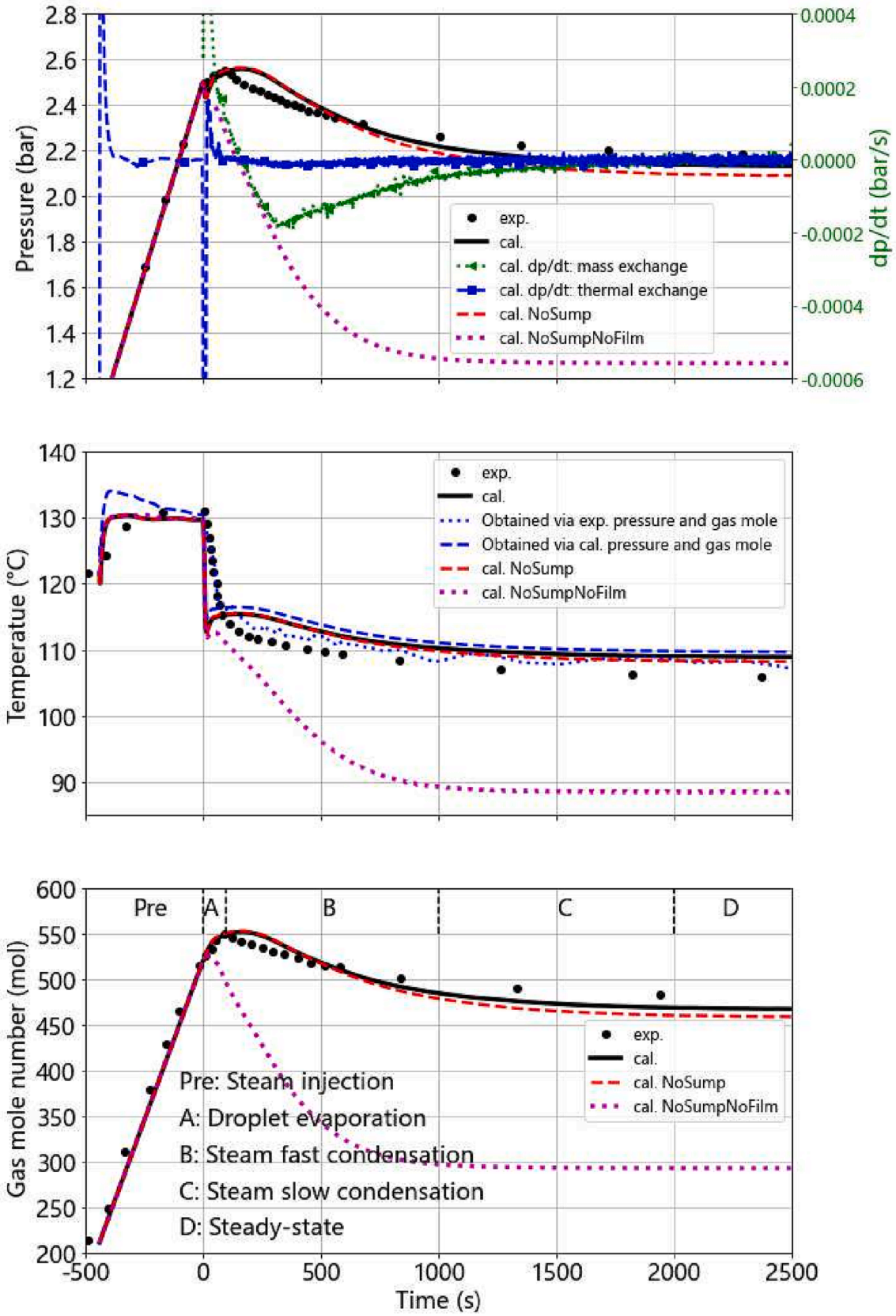

Fig. 10. Pressure, average temperature, gas mole number and depressurization contributions.

thermal couples installed in the test vessel. Due to a lack of information on the exact locations of the thermal couples, the arithmetic mean value of the calculated temperature in each computational cell was used. The comparison demonstrates the deviation due to the temperature stratification, as seen in Fig. 12 and Fig. A3 in the supplementary data, which show that the gas temperature distribution is quite heterogeneous in the axial vertical direction. Another two average temperatures obtained via the experimental and calculated pressure and total gas mole number (by the ideal gas equation $T = \frac{pV}{nR}$) are plotted in Fig. 10 blue curves, which agree well with the GASFLOW prediction (black curve), comparing the deviation between the experimental data (black dots) and the GASFLOW prediction at the beginning of the spray.

Fig. 11 presents the time evolution of the local gas temperature after spraying (upper subfigure) and the radial profile of the gas temperature (lower subfigure) at 600 s and at the final equilibrium at a height of 2.04 m on the TOSQAN central axis, directly above the steam release location. The calculated local temperature is in good agreement with the experimental data, with a decreasing trend similar to the mean temperature in the facility, ranging from 127 °C to 105 °C. The radial profile of the temperature indicates no significant temperature gradient in the horizontal direction. While there is clear thermal stratification along the vertical axis, the temperature is quite homogeneous horizontally.

4.3.3. *Effect of water droplets and film evaporation*

The wall temperature was kept constant at approximately 120 °C throughout the entire test. Accurately predicting the spray-wall interaction and water evaporation on the hot walls is of great importance for the success of the numerical simulation. The evaporation rate of the spray-formed film is determined by the film heat transfer coefficient, which depends on the flow pattern of the spray droplets attaching to walls and forming rivulets and films (Wang and Zhao, 2021). Although the evaporation of the water droplets was well-predicted at the beginning of the spray, the evaporation of the film and sump on walls at the temperature of 120 °C in the following phase is significant. Cases without sump and film evaporation have been conducted for comparison purposes, as seen in Fig. 10. It shows that without taking film evaporation into account, the pressure, temperature, and amount of gas species decrease significantly, reaching 1.26 bar, 88 °C, and 295 mol at the equilibrium state. This indicates that the contribution of water film evaporation on the walls to the total amount of gas is roughly 40%.

At the very beginning of the spray (0–6 s), the water droplets at 119 °C cool down the steam at 127 °C in the upper part of the vessel, and the pressure decreases because the amount of vaporized water cannot compensate for the heat losses. When the water droplets move to the lower part of the vessel, strong evaporation occurs in this region with a temperature of 162 °C and a steam volume fraction of 30%. The temperature of the droplet surface is reduced to around 70 °C due to the evaporation. When the water droplets arrive at the bottom of the vessel where the initial gas temperature and steam volume fraction are 125 °C and 5%, very strong evaporation occurs, including the water droplets' evaporation in the dry hot gas mixtures, as well as the water film evaporation on the hot walls. As shown in Fig. 10, it seems that the

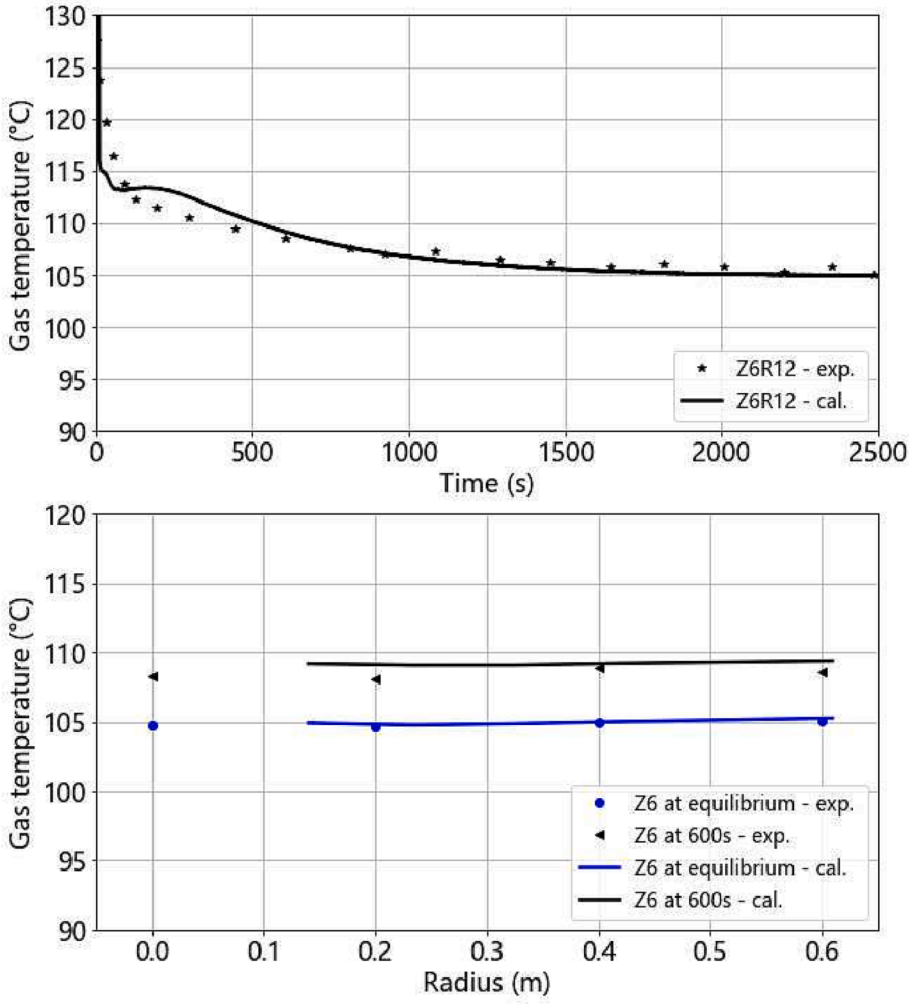

Fig. 11. Gas temperature and radius distribution on height Z6.

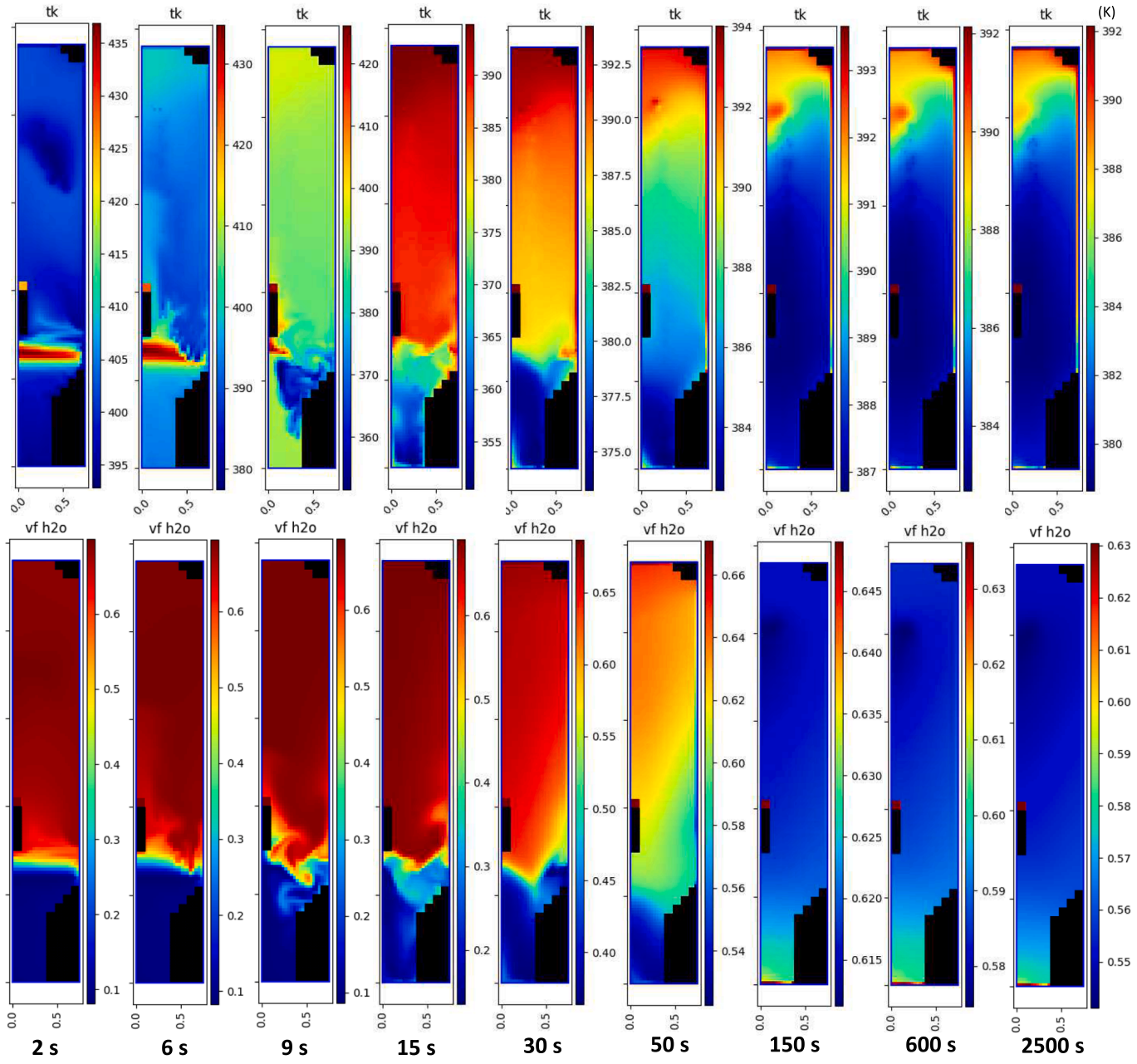

Fig. 12. Gas temperature and steam volume fraction development.

evaporation on the solid hot walls dominates the pressure increase and steam generation from 6 s to 150 s because the pressure and amount of steam decrease rapidly without considering the film evaporation. This detailed pressure evolution has not been revealed and discussed in previous researches (Ding et al., 2017; Malet et al., 2011a; Malet et al., 2011; Mimouni et al., 2010). This study assumes that the water film uniformly covers the surface of the wall. The water coverage area could be smaller in reality if rivulets are formed on walls. That is why the calculated pressure is slightly larger than the experimental data from 100 s to 500 s. The effect of rivulets on the water evaporation rate is worthy of further investigation. After 500 s, the gas temperature and total steam mass decrease slowly due to the cooling of the injected water droplets, and an equilibrium state (2.2 bar and 110 °C) is gradually established in the vessel when the heat extracted by the water droplets is balanced by the energy supplied from the hot walls. This shows that the initial conditions before the spray injection and the water evaporation on the hot walls are of great importance for the containment thermohydraulics.

5. Conclusions

The spray system is considered to be an effective measure to prevent overpressure and enhance hydrogen mixing with the air–steam mixtures in the nuclear containment during hypothetical severe accidents. To enable 3D thermal–hydraulic analysis with the spray system in full-scale engineering applications, an efficient Eulerian-Lagrangian modeling approach has been developed in the CFD code GASFLOW, which has the following features:

1) Two-way coupling of mass, momentum, energy, and turbulence between the continuous gas and discrete water droplets.

2) A group of water droplets, enabling efficient 3D simulations of full-scale reactor containment.
3) Heat and mass transfer between each group of water droplets and the surrounding gas.
4) Droplet-wall interaction and static water film evaporation on solid walls.
5) Droplet generation with droplet size and velocity distribution, and various spray shapes according to engineered spray nozzles.

The models have been validated using the TOSQAN spray experiments, which investigate the effects of the spray droplet swarm on the continuous gas phase.

- The TOSQAN 113 test was used mainly to validate two-way momentum coupling between gas mixtures and spray droplets, investigating gas mixing and the break-up of helium stratification due to spray droplet movement. Gas entrainment erodes helium stratification both upwards and downwards due to diffusion and convection, respectively. The spray droplet swarm maintains a cone shape only at the nozzle outlet; however, it is highly influenced by the development of the velocity vector and gas entrainment. Droplet size distribution and spray shape analysis indicate that using multiple droplet sizes following a log-normal distribution yields better results than using geometry or Sauter mean diameter. Smaller droplets result in more intense gas mixing. The spray shape has a significant impact on the dynamic and thermodynamic effect on the atmosphere.
- The TOSQAN 101 test was used to validate two-way mass and energy couplings between the continuous and discrete phases, studying atmosphere depressurization due to heat and mass transfer. The results showed good agreement between calculated and experimental data, with deviations under 10%. Steam mass and thermal exchange caused by the spray jointly determine containment pressure, with mass exchange dominating the depressurization rate. Water film evaporation contributes roughly 40% to the total gas, and pressure evolution due to film evaporation on hot walls dominates steam generation. The study highlights the importance of initial temperature and steam concentration distribution for predicting the early phase and the correct calculation of water droplets and film evaporation on solid walls for the entire successful simulation. Investigations are needed to understand the uncertainties and the effects of flow patterns of spray-formed film/rivulet on walls.

The newly developed GASFLOW offers the capability to investigate 3D thermal–hydraulic phenomena by integrating the Eulerian-Lagrangian approach with film/structure heat transfer mechanisms. Significantly, this tool exhibits promise in modeling a range of complex scenarios, such as the impact of spray on containment depressurization, hydrogen distribution, and radioactive aerosol wash-out in full-scale containment.

Declaration of Competing Interest

The authors declare that they have no known competing financial interests or personal relationships that could have appeared to influence the work reported in this paper.

Data availability

Data will be made available on request.

References

Abramzon, B., Sirignano, W.A., 1989. Droplet vaporization model for spray combustion calculations. Int. J. Heat Mass Transf. 32 (9), 1605–1618.

Amani, E., Nobari, M.R.H., 2013. A calibrated evaporation model for the numerical study of evaporation delay in liquid fuel sprays. Int. J. Heat Mass Transf. 56 (1–2), 45–58.

Babić, M., Kljenak, I., Mavko, B., 2009. Simulations of TOSQAN containment spray tests with combined Eulerian CFD and droplet-tracking modelling. Nucl. Eng. Des. 239 (4), 708–721.

Clift, R., Grace, J.R., Weber, M.E., 1978. Bubbles, drops, and particles.

Ding, P., Liu, Y., Wang, B., Li, W., Wang, J., 2017. The homogeneous and Lagrangian tracking approaches of the spray simulation in the containment. Ann. Nucl. Energy 101, 203–214.

Erkan, N., Kapulla, R., Mignot, G., Zboray, R., Paladino, D., 2011. Experimental investigation of spray induced gas stratification break-up and mixing in two interconnected vessels. Nucl. Eng. Des. 241 (9), 3935–3944.

Foissac, A., Malet, J., Vetrano, M.R., Buchlin, J.-M., Mimouni, S., Feuillebois, F., Simonin, O., 2011. Droplet size and velocity measurements at the outlet of a hollow cone spray nozzle. Atomizat. Sprays 21 (11), 893–905.

Foissac, A., Malet, J., Mimouni, S., Ruyer, P., Feuillebois, F., Simonin, O., 2013. Eulerian simulation of interacting PWR sprays including droplet collisions. Nucl. Technol. 181 (1), 133–143.

Gosman, A.D., loannides, E., 1983. Aspects of computer simulation of liquid-fueled combustors. J. Energy 7 (6), 482–490.

Gunn, R., Kinzer, G.D., 1949. The terminal velocity of fall for water droplets in stagnant air. J. Atmospheric Sci. 6 (4), 243–248.

Gupta, S., Schmidt, E., Freitag, M., Langerock, G. and Funke, F., 2017, May. Experimental investigations on containment spray performance under severe accident conditions. In Proceedings of 8th European Review Meeting on Severe Accident Research (ERMSAR), Warsaw, Poland.

IAEA, 2011. Mitigation of Hydrogen Hazards in Severe Accidents in Nuclear Power Plants. IAEA TECDOC-1661, International Atomic Energy Agency, Vienna, p. 2011.

Kim, J., Lee, U., Hong, S.-W., Kim, S.-B., Kim, H.-D., 2006. Spray effect on the behavior of hydrogen during severe accidents by a loss-of-coolant in the APR1400 containment. Int. Commun. Heat Mass Transfer 33 (10), 1207–1216.

Lemaitre, P., Nuboer, A., Porcheron, E., 2005. TOSQAN Experimental Programme, Spray test no 101. Technical report, DSU/SERAC/LECEV/05-11 (IRSN 91192 Gifsur Yvette, France).

Malet, J., Blumenfeld, L., Arndt, S., Babic, M., Bentaib, A., Dabbene, F., Kostka, P., Mimouni, S., Movahed, M., Paci, S., Parduba, Z., Travis, J., Urbonavicius, E., 2011. Sprays in containment: final results of the SARNET spray benchmark. Nucl. Eng. Des. 241 (6), 2162–2171.

Malet, J., Lemaitre, P., Porcheron, E., Vendel, J., Bentaib, A., Plumecocq, W., Dumay, F., Chin, Y.C., Krause, M., Blumenfled, L. and Dabbene, F., 2005, November. Modelling of sprays in containment applications: results of the TOSQAN spray benchmark (Test 101). In Proceedings of The First European Review Meeting on Severe Accident Research, ERSMAR-2005, Aix-en-Provence, France.

Malet, J., Gelain, T., Mimouni, S., Manzini, G., Arndt, S., Klein-Hessling, W., Xu, Z., Povilaitis, M., Kubisova, L., Parduba, Z. and Paci, S., 2011a. Spray model validation on single droplet heat and mass transfers for containment applications-SARNET-2 benchmark. The 14th International Topical Meeting on Nuclear Reactor Thermalhydraulics, September 25-30th, 2011, Toronto, Canada.

Malet, J., Huang, X., 2015. Influence of spray characteristics on local light gas mixing in nuclear containment reactor applications. Comput. Fluids 107, 11–24.

Mimouni, S., Lamy, J.S., Lavieville, J., Guieu, S., Martin, M., 2010. Modelling of sprays in containment applications with a CMFD code. Nucl. Eng. Des. 240 (9), 2260–2270.

Movahed, M. A., and J. R. Travis. "Assessment of the GASFLOW spray model based on the calculations of the TOSQAN experiments 101 and 113." In CFD4NRS-3: Experimental Validation and Application of CFD and CMFD Codes to Nuclear Reactor Safety Issues OECD/NEA & IAEA Workshop Hosted by United States NRC Washington DC, USA, pp. 14-16. 2010.

Movahed, M., Eyink, J., Travis, J., 2005. Effect of spray activation on the reactivity of the hydrogen–air–steam mixture in the containment of the European Pressurized Water reactor (EPR). In: Proceedings of the 11th International Topical Meeting on Nuclear Reactor Thermal-hydraulics, NURETH-11, Avignon, France.

OECD, 1999. State of the art report on containment thermahydraulics and hydrogen distribution. OECD Report, France.

OECD, 2012. OECD/SETH-2 project PANDA and MISTRA experiments final summary report. Investigation of key issues for the simulation of thermal-hydraulic conditions in water reactor containment. OECD Report, France.

Oseen, C.W., 1910. Uber die Stokes' sche Formel und Uber eine verwandte Aufgabe in der Hydrodynamik. Arkiv Mat., Astron. och Fysik 6, 1.

Plumecocq, W., Passalacqua, R., 2001. Status of emergency spray modelling in the integral code ASTEC. Proceedings of the 9th international conference on nuclear engineering, ICONE-9, April 8-12, 2001, Palais des congres Acropolis, Nice, France.

Porcheron, E., Thause, L., Malet, J., Cornet, P., Brun, P., Vendel, J., 2002. simultaneous application of spontaneous Raman scattering and LDV/PIV for steam/air flow characterization. In 10th International symposium on flow visualization, Kyoto, Japan (pp. 26-29).

Porcheron, E., Lemaitre, P., Nuboer, A., Rochas, V., Vendel, J., 2007. Experimental investigation in the TOSQAN facility of heat and mass transfers in a spray for containment application. Nucl. Eng. Des. 237 (15–17), 1862–1871.

Putnam, A., 1961. Integratable form of droplet drag coefficient. Ars J. 31 (10), 1467–1468.

Rabe, C., Malet, J., Feuillebois, F., 2010. Experimental investigation of water droplet binary collisions and description of outcomes with a symmetric Weber number. Phys. Fluids 22 (4), 047101.

Ranz, W.E., Marshall, W.R., 1952. Evaporation from drops: Part I & II. Chem. Eng. Prog 48, 173–180.

Royl, P., Rochholz, H., Breitung, W., Travis, J., Necker, G., 2000. Analysis of steam and hydrogen distribution with PAR mitigation in NPP containments. Nucl. Eng. Des. 202, 231–248.

Schiller, L., Naumann, A., 1935. A drag coefficient correlation. Z. Ver. Dtsch. Ing. 1935 (77), 318–320.

Spalding, D.B., 1953. The combustion of liquid fuels. Symp. (Int.) Combust. 4 (1), 847–864.

Strizhak, P.A., Volkov, R.S., Castanet, G., Lemoine, F., Rybdylova, O., Sazhin, S.S., 2018. Heating and evaporation of suspended water droplets: Experimental studies and modelling. Int. J. Heat Mass Transf. 127, 92–106.

Subki, H., 2020. Advances in small modular reactor technology developments. A supplement to: advanced reactors information system (ARIS), IAEA.

Wang, F., Xiao, J., Jordan, T., 2023. Extension of spray droplet/aerosol heat transfer model in containment atmosphere under severe accident. Annals of Nuclear Energy, Under review.

Wang, F., Zhao, M., 2021. Behavior of moving droplet on inclined containment wall: Experiment and model validation. Nucl. Eng. Des. 376.

Wang, F., Zou, Z., Deng, J., Qin, H., Zhang, M., 2022. Investigations of hydrogen hazard mitigation by deliberate ignition in small modular reactor during severe accident using GASFLOW-MPI. Ann. Nucl. Energy 179.

Whang, S., Park, H.S., Kim, J., 2021. In-depth analysis of mixing characteristics of stratified gases during spray operation in the TOSQAN Test 113 using OpenFOAM. Nucl. Eng. Des. 373.

Xiao, J., Travis, J.R., Royl, P., Necker, G., Svishchev, A. and Jordan, T., 2016 b. GASFLOW-MPI: A scalable computational fluid dynamics code for gases, aerosols and combustion", Volume 1: Theory and Computational Model (Revision 1.0), ISBN 978-3-7315-0448-1, Karlsruhe Institute of Technology (KIT), Germany.

Xiao, J., Travis, J.R., Royl, P., Necker, G., Svishchev, A., Jordan, T., 2016. Three-dimensional all-speed CFD code for safety analysis of nuclear reactor containment: Status of GASFLOW parallelization, model development, validation and application. Nucl. Eng. Des. 301, 290–310.

Yuen, M.C., Chen, L.W., 1976. On drag of evaporating liquid droplets. Combust. Sci. Technol. 14 (4–6), 147–154.

Zhifu, Z., Guoxiang, W., Bin, C., Liejin, G., Yueshe, W., 2013. Evaluation of evaporation models for single moving droplet with a high evaporation rate. Powder Technol. 240, 95–102.

Zou, Z., Wang, F., Deng, J., Zhang, H., Zhang, M., Peng, H., Wang, X., Qin, H., 2022. Hydrogen hazard mitigation in small modular reactor during SBO severe accident using GASFLOW-MPI. Prog. Nucl. Energy 147 (2022), 104193.